

Josephson diode and spin-valve effects on the surface of altermagnet CrSb

V.D. Esin,¹ D.Yu. Kazmin,¹ Yu.S. Barash,¹ A.V. Timonina,¹ N.N. Kolesnikov,¹ and E.V. Deviatov^{1,2}

¹*Institute of Solid State Physics of the Russian Academy of Sciences,
Chernogolovka, Moscow District, 2 Academician Ossipyan str., 142432 Russia*

²*V.L. Ginzburg Research Centre for High-Temperature Superconductivity and Quantum Materials,
P.N. Lebedev Physical Institute of RAS, Moscow 119991, Russia*

(Dated: February 10, 2026)

We experimentally investigate charge transport in In-CrSb and In-CrSb-In proximity devices, which are formed as junctions between superconducting indium leads and thick single crystal flakes of altermagnet CrSb. For double In-CrSb-In junctions, the obtained $dV/dI(B)$ curves are mirrored in respect to zero field for two magnetic field sweep directions, which is characteristic behavior of a Josephson spin valve. Also, we demonstrate Josephson diode effect by direct measurement of the critical current for two opposite directions in external magnetic field. We interpret these observations as a joint effect of the spin-polarized topological surface states and the altermagnetic spin splitting of the bulk bands in CrSb. For a single In-CrSb interface, the superconducting gap oscillates in magnetic field for both field orientations, which strongly resembles the transition into the Fulde-Ferrell-Larkin-Ovchinnikov (FFLO) state. The latter is based on finite-momentum Cooper pairing against a background of the Zeeman splitting, so it fully compatible with the requirements for the Josephson diode effect.

PACS numbers: 73.40.Qv 71.30.+h

I. INTRODUCTION

In altermagnets, the concept of spin-momentum locking^{1,2} was extended to the case of weak spin-orbit coupling, i.e. to the non-relativistic groups of magnetic symmetry^{3,4}. As a result, the small net magnetization is accompanied by alternating spin-momentum locking in the k -space, so the unusual k -dependent spin splitting is predicted^{3,5,6}. In the simplest case of d-wave symmetry, the up-polarized subband can be obtained by $\pi/2$ rotation of the down-polarized one in the k -space^{7,8}. Consequently, an altermagnet sometimes behaves as an antiferromagnet, and sometimes as a ferromagnet, depending of the crystal-field or interface-crystal relative orientations.

There are many theoretical predictions on possible effects of proximity-induced superconductivity in altermagnets^{6,7,9–19}. For example, as the direct consequence of k -dependent spin splitting, orientation-dependent effects can be expected for different superconductor-altermagnet-superconductor^{6,14} (SNS) and superconductor-altermagnet^{9,15–17,19,20} (SN) structures. For applications, the absence of stray fields in altermagnets makes them advantageous for superconducting spintronics logic circuits.

Spin-momentum locking is a key feature not only of altermagnets, but also of a large class of topological materials¹. In the latter case, it is responsible for the spin polarization of the topological surface states²¹, which are able to carry supercurrents over extremely large distances^{22–26}. Weyl semimetal states have also been theoretically proposed in altermagnets^{27,28}. Spin-polarized surface states can lead to the different realizations of the Josephson diode effect (JDE) in proximity topological devices.

The diode effect in superconductors occurs if the criti-

cal current I_c is different for two opposite directions. For the Josephson diode effect, the absolute values of $I_c^+(B)$ (positive I_c) and $I_c^-(B)$ (negative I_c) differ for the two current sweep directions (nominally + and - ones). This behavior should be distinguished from usual difference between the critical and the return currents owing to the finite capacitance of devices, while JDE emerges under certain conditions in systems with broken time-reversal and inversion symmetries^{9,29–38}.

As possible physical mechanisms of JDE, Cooper pairs can acquire a finite momentum and give rise to a diode effect in superconductors with strong spin-orbit coupling^{39–41}. In paramagnetic and centrosymmetric Dirac semimetal NiTe_2 , the finite momentum pairing results from the momentum shift of topological surface states under an in-plane magnetic field due to the spin-momentum locking^{30,31}. In superconducting heterostructures with non-coplanar magnetization textures, breaking the magnetization reversal symmetry can result in the direct coupling between the magnetic moment and the supercurrent, and, therefore, in the Josephson diode effect^{42–47}.

Also, the Josephson diode effect is typically observable for Josephson spin-valves (JSV), where the ferromagnetic multilayer^{48,49} is sandwiched between two superconducting electrodes in vertical^{50–57} or planar geometries⁵⁸. While in conventional Josephson junctions supercurrent is modulated by magnetic flux, in a Josephson spin valve it is mainly controlled by the relative orientation of magnetic layers, giving rise to the critical current asymmetry and reversal. A Josephson spin valve can also be realized on the surface of the proximized magnetic topological semimetal²⁹. Spin-polarized surface states and a ferromagnetic bulk can be considered as two spin-polarized layers^{48,49}, so the magnetic topological materials demonstrate spin-valve transport properties^{59–62}. The Joseph-

son spin-valve behavior has recently been observed in Nb-Mn₃Ge-Nb junctions containing a single interlayer of the topological chiral antiferromagnet Mn₃Ge⁶³.

The Josephson diode effect has recently been predicted for junctions incorporating altermagnets^{9,64-66}. Experimental investigations of the Josephson current asymmetry can be conveniently performed for CrSb, which has recently been identified as a new altermagnetic metal through spin-integrated soft X-ray angular-resolved photoelectron spectroscopy (SX-ARPES)⁶⁷. In contrast to the well-known altermagnet MnTe⁶⁸⁻⁷⁰, spin-orbit coupling plays a minor role in the low energy band structure in CrSb, so the altermagnetism is well defined and characterized by non-relativistic spin-group symmetries⁷¹. Also, CrSb metal is of high bulk conductance even at low temperatures, which facilitates fabrication of transparent SN interfaces for the altermagnetic-based proximity devices in comparison with the semiconductor MnTe²⁰.

CrSb reveals both altermagnetic and topological features⁷². The altermagnetic band spin splitting has been clearly demonstrated along with signature of topological surface states on the (100) cleaved side surface close to the Fermi level originating from bulk band topology in CrSb⁷³. It was confirmed by observation of the interplay between the altermagnetic bulk and the topological surface magnetizations for CrSb⁷⁴. Thus, it is reasonable to investigate possible anomalies in Josephson effect induced by these surface states for the altermagnetic candidate CrSb.

Here, we experimentally investigate charge transport in In-CrSb and In-CrSb-In proximity devices, which are formed as junctions between superconducting indium leads and thick single crystal flakes of altermagnet CrSb. For double In-CrSb-In junctions, the obtained $dV/dI(B)$ curves are mirrored in respect to zero field for two magnetic field sweep directions, which is characteristic behavior of a Josephson spin valve. Also, we demonstrate Josephson diode effect by direct measurement of the critical current for two opposite directions in external magnetic field. For a single In-CrSb interface, the superconducting gap oscillates in magnetic field for both field orientations, before its full suppression.

II. SAMPLES AND TECHNIQUE

CrSb single crystals were synthesized by reaction of elements. Cr (99.996%) and Sb (99.9999%) were mixed in the stoichiometric ratio and then heated in an evacuated silica ampule up to 1000°C with the rate of 15°C/h in a gradient-free furnace. The load was held at 1000°C for 72 hours and then cooled down slowly (11°C/h) to the room temperature. The crystals grown are faceted single crystals with the space group $P6_3/mmc$ No. 194 and the stoichiometric composition, as confirmed by X-ray diffraction analysis, see Fig. 1.

The images in Fig. 1(a) shows schematically sample fabrication. CrSb is a three-dimensional altermagnet, so

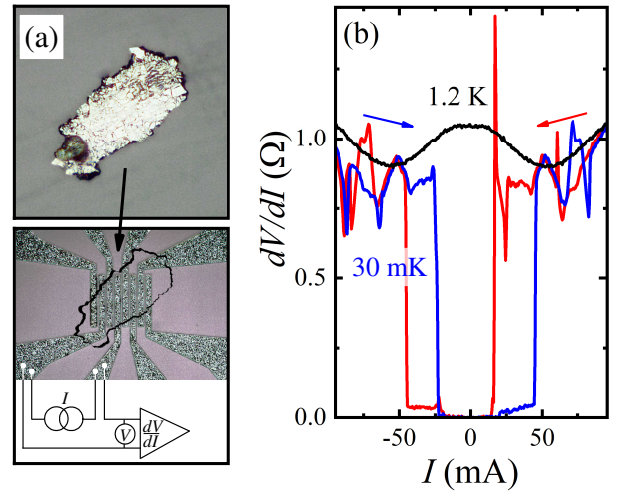


FIG. 1. (Color online) (a) Optical image of the CrSb single-crystal flake (top image), which is placed on the pre-defined In leads pattern (the bottom one) to form 2 μm separated In-CrSb junctions. To investigate Josephson current through the CrSb surface, In-CrSb-In resistance is measured in a standard four-point technique. (b) Josephson $dV/dI(I)$ curves at 30 mK temperature, the blue and the red curves are for two opposite current sweep directions, respectively. Zero-resistance state can be clearly seen, which is accompanied by usual hysteresis for the critical and the return currents. The black curve demonstrates suppression of the Josephson effect at 1.2 K. The curves are obtained after sample cooling in zero magnetic field, before any sample magnetization.

one has to select relatively thick (above 1 μm) single crystal flakes. The desired experimental geometry can not be defined by usual mesa etching for the well-conducting CrSb single crystals. Instead, the contacts are formed by pre-defined indium leads pattern on a standard Si/SiO₂ substrate.

The 5 μm wide In leads are separated by 2 μm intervals, as depicted in Fig. 1 (a), they are formed by lift-off technique after thermal evaporation of 100 nm In. CrSb single crystal flakes are obtained by mechanical exfoliation. We select the most plane-parallel flakes with the $\approx 100 \mu\text{m}$ lateral size. The chosen flake is placed immediately on the In contact leads. After initial single-shot pressing by another oxidized silicon substrate, the flake is firmly connected to the In leads. This procedure provides transparent In-CrSb junctions (about 1 Ohm normal resistance), stable in different cooling cycles, which has been verified before for a wide range of materials^{25,29,75,76}. As an additional advantage, the In-CrSb interfaces are protected from any contamination by CrSb bulk and the Si/SiO₂ substrate.

Every In-CrSb junction can be independently characterized in a three-point connection scheme: one In contact is grounded, the neighbor (2 μm separated) In contact is used as a voltage probe, while current is fed through another (remote) contact. We use an addi-

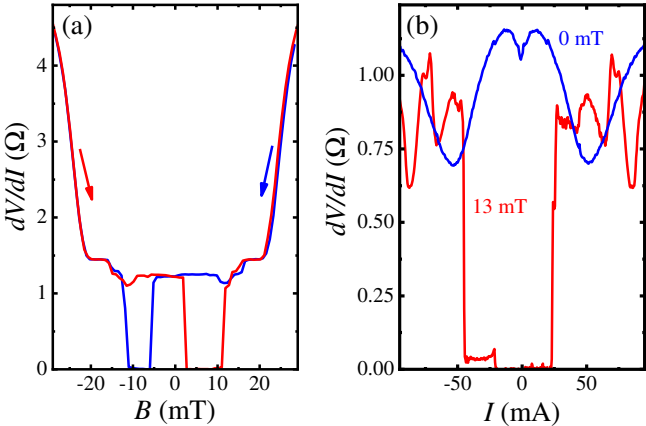


FIG. 2. (Color online) (a) Josephson spin-valve effect as the $dV/dI(B)$ curves reversal for two opposite magnetic field sweep directions. After magnetization of the sample, the zero-resistance region is not only shifted to finite magnetic fields, but the $dV/dI(B)$ curves are mirrored in respect to zero field, including regions with finite resistance. (b) $dV/dI(I)$ curves after magnetization of the sample. Differential resistance is always finite at zero field now, but there is wide zero-resistance region at 13 mT magnetic field. Magnetic field is directed normally to the In-CrSb interfaces (i.e. to the CrSb flake), the data are obtained at 30 mK temperature.

tional (fourth) wire to the grounded contact, so all the wire resistances are excluded, which is necessary for low-impedance samples. If there is no supercurrent between two neighbor In leads, the potential probe mostly reflects the voltage drop across the grounded junction^{23,31}, i.e. the Andreev reflection^{77,78} at the In-CrSb interface. Otherwise, if the potential probe shows exactly zero for some current range, the two neighbor In leads are connected by the Josephson current. In the latter case, the In-CrSb-In resistance is measured in a standard four-point technique^{25,29,31,75,76}, as schematically presented in Fig. 1 (a).

To obtain differential $dV/dI(V)$ and $dV/dI(I)$ characteristics, dc current is additionally modulated by a low (100 nA) ac component, so the lock-in detected ac voltage is proportional to the differential resistance $\sim dV/dI$. The signal is confirmed to be independent of the modulation frequency within 100 Hz – 10 kHz range, which is defined by the applied filters. The measurements below are performed for 30 mK and 1.2 K temperatures in a dilution refrigerator.

III. EXPERIMENTAL RESULTS

A. Double In-CrSb-In junctions

For two transparent neighbor In-CrSb junctions, Josephson current connects the indium leads, see Fig. 1 (b). The zero-resistance region is slightly asymmetric for every current sweep direction, so there is usual hystere-

sis for the critical and the return currents. The current range is much below the critical current of the indium leads, which we can estimate for our leads' dimensions as about 30 mA for the known⁷⁹ value $j \approx 3 \times 10^6$ A/cm².

Josephson current is suppressed at 1.2 K temperature in Fig. 1 (b), so the $dV/dI(I)$ curve is of standard Andreev shape⁷⁸ with two resistance minima at $\approx \pm 0.5$ mA current bias. While the normal resistance value is $\approx 1\Omega$ in Fig. 1 (b), the superconducting gap can be estimated as 0.5 mA $\times 1\Omega \approx 0.5$ meV, which well corresponds to the bulk indium gap⁸⁰.

The curves in Fig. 1 (b) are obtained after sample cooling in zero magnetic field, before any sample magnetization. Fig. 2 (a) shows the effect of the magnetic field for two opposite field sweep directions. After sample magnetization at ± 100 mT magnetic field, the zero-resistance regions are shifted to finite fields $\approx \pm 10$ – 13 mT, as confirmed by the $dV/dI(I)$ curves in Fig. 2 (b): the differential resistance is finite at zero field value, but there is zero-resistance region at 13 mT magnetic field. The field is directed normally to the In-CrSb interfaces (i.e. to the CrSb plane), the values are well below the indium critical field (110 mT for the 100 nm thick films⁸⁰, which we confirm for our indium leads). Also, there is no noticeable frozen flux for this field range for our solenoid.

The main experimental finding is the $dV/dI(B)$ curves reversal in Fig. 2 (a). Indeed, for two magnetic field sweep directions, the $dV/dI(B)$ curves are mirrored in respect to zero field, including regions with finite dV/dI differential resistance. The observed behavior is known for Josephson spin valves^{29,63}.

The spin-valve effect is not so strong in parallel to the In-CrSb interfaces magnetic field orientation, see Fig. 3. Before magnetization of the sample, $dV/dI(I)$ curves in Fig. 3 (a) well reproduce those from Fig. 1 (b): the zero-resistance region is slightly asymmetric for every current sweep direction, it is suppressed at 1.2 K temperature in Fig. 3 (a). After magnetization of the sample, the $dV/dI(B)$ curves are clearly mirrored in respect to zero field (see also the regions of finite resistance), confirming the Josephson spin-valve behavior. Thus, the spin-valve effect is sensitive to the $\pi/2$ rotation of the magnetic field, which resembles the results for CrSb magnetization⁷⁴.

Since the Josephson spin valves usually demonstrate the Josephson diode effect^{29–31}, we show the $I_c^+(B)$ and the inverted $-I_c^-(B)$ critical current values in the inset to Fig. 3 (b). The Josephson critical current I_c^\pm is measured for the transition from the superconducting $dV/dI = 0$ state to the resistive $dV/dI > 0$ state for the positive and negative dc currents (i.e. for + and - current sweep directions). Since the transition from the superconducting to resistive states is stochastic, to obtain I_c with high accuracy, we sweep the dc current ten times from zero value to some value well above the critical current I_c at fixed B and then determine I_c for this field B as an average value of dV/dI breakdown positions. The obtained $I_c^\pm(B)$ curves are asymmetric in respect to zero magnetic field in the inset to Fig. 3 (b), but they coincide

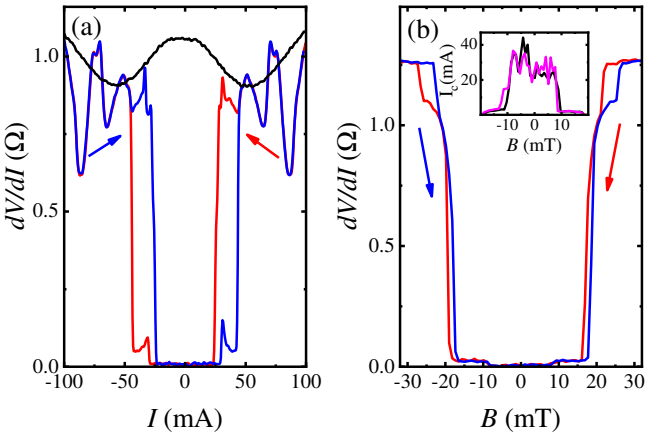


FIG. 3. (Color online) Josephson spin-valve effect for the parallel to the In-CrSb interfaces magnetic field orientation at 30 mK temperature. (a) Before magnetization of the sample, $dV/dI(I)$ curves well reproduce ones from Fig. 1 (b). The zero-resistance region is slightly asymmetric for every current sweep direction (red and blue curves), it is suppressed at 1.2 K temperature (the black one). (b) After magnetization of the sample, the $dV/dI(B)$ curves are mirrored in respect to zero field (see also the regions of finite resistance), confirming the Josephson spin valve behavior. Inset shows the Josephson diode effect as another demonstration of the $dV/dI(B)$ curves reversal: the measured critical currents $I_c^\pm(B)$ are asymmetric in respect to zero field, but they coincide well when drawn as $I_c^+(B)$ (positive I_c) and $-I_c^-(B)$ (the inverted negative I_c for the inverted field value)^{29–31}.

only when drawn as $I_c^+(B)$ (positive I_c) and $-I_c^-(B)$ (the inverted negative I_c for the inverted field value), which is the direct demonstration of the Josephson diode effect^{29–31}.

As a result, double In-CrSb-In not only transfer Josephson current at millikelvin temperatures on the surface of altermagnet CrSb, but also demonstrate prominent Josephson spin-valve and diode behavior in external magnetic field.

B. Single In-CrSb junction

As prepared, the In-CrSb interface transparency varies from junction to junction. For some neighbor In probes the superconducting order parameter is suppressed along the CrSb surface at distances smaller than $2\mu\text{m}$ probe separation. In this case, we can use the three-point connection scheme to investigate differential resistance of a single (grounded) In-CrSb junction, as described in the Samples section.

The typical $dV/dI(V)$ curve is presented in Fig. 4 (a). We have verified that for a fixed grounded In contact, the obtained $dV/dI(V)$ curves are independent of the mutual positions of current/voltage probes, so they indeed reflect the resistance of In-CrSb interface without any noticeable admixture of the CrSb bulk resistance. Due to these

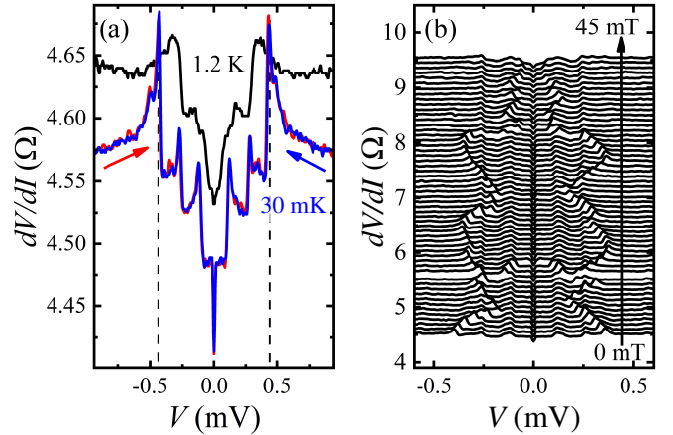


FIG. 4. (Color online) Andreev behavior of dV/dI differential resistance for a single In-CrSb junction. (a) $dV/dI(V)$ curves in zero magnetic field at two different temperatures, 30 mK and 1.2 K, respectively. Differential resistance is diminished within $\approx \pm 0.5$ mV bias interval (depicted by vertical dashed lines). Temperature has low effect on $dV/dI(V)$ curve, however, the zero-bias anomaly disappears at 1.2 K, as well as the fine subgap structures. (b) Magnetic field suppression of Andreev reflection as a waterfall plot (i.e., the $dV/dI(V)$ curves are shifted vertically). As expected, the superconducting gap is suppressed by magnetic field, but the suppression is non-monotonic: the gap oscillates with ≈ 13 mT period. The curves are obtained at 30 mK temperature for the parallel to the In-CrSb interface magnetic field.

considerations, we should analyze Fig. 4 (a) in terms of Andreev reflection at single NS interface.

Since Andreev reflection allows subgap transport of Cooper pairs, it appears experimentally as the resistance drop for voltages within the superconducting gap^{77,78}. As it can be seen in Fig. 4 (a), differential resistance is reduced over a certain bias interval (see the vertical dashed lines), which is a bit smaller than the known 0.5 mV bulk indium gap⁸⁰. The partial gap suppression can be expected due to the finite spin polarization of the CrSb altermagnet surface, as it is supported by Josephson diode effect observation in Figs. 2 and 3.

The indium is always superconducting for our 30 mK – 1.2 K dilution fridge temperature range. Thus, temperature has low effect on the width of the differential resistance drop in Fig. 4 (a), so the superconducting gap is only somewhat diminished at 1.2 K. However, the zero-bias anomaly disappears, as well as the fine subgap structures which are well developed at 30 mK.

Since Andreev process is defined by the superconducting gap, it should be monotonically suppressed by magnetic field^{77,78}. The evolution of the $dV/dI(V)$ curve in magnetic field is shown in Fig. 4 (b) as a waterfall plot. The superconducting gap, determined as the full width of the differential resistance drop, is indeed suppressed by magnetic field, but the suppression is non-monotonic: the gap oscillates in the external field with ≈ 13 mT period, which well correlates with the shift of the zero-resistance

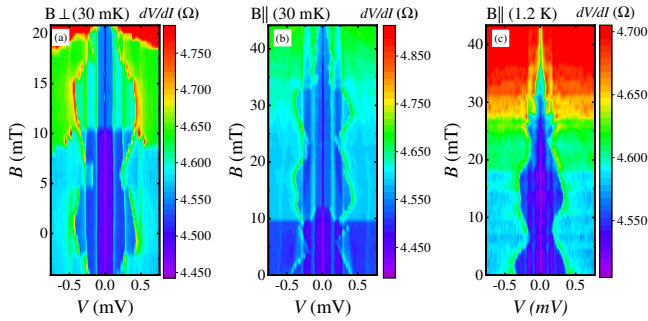


FIG. 5. (Color online) Non-monotonic behavior of the proximized superconductivity on the surface of altermagnet CrSb as the detailed colormaps of $dV/dI(B, V)$ differential resistance at 30 mK temperature for two, normal (a) and in-plane (b), magnetic field orientations, respectively, and at 1.2 K for the in-plane field in (c). The superconducting gap oscillates for both field orientations with similar ≈ 13 mT period in (a) and (b), while it is suppressed earlier in normal to the In-CrSb interface magnetic field. The oscillations with the same period survive even at 1.2 K in (c).

region in Fig. 2 (b). In contrast, the subgap structures are stable in magnetic field in Fig. 4 (b).

The detailed picture of the gap suppression is shown in Fig. 5 (a-c) for two magnetic field orientations and two, 30 mK and 1.2 K, temperatures. The superconducting gap oscillates for both field orientations with similar ≈ 13 mT period, compare Figs. 5 (a) and (b), while the gap is suppressed earlier in normal to the In-CrSb interface magnetic field. The oscillations with the same period survive even at 1.2 K in Fig. 5 (c) for the in-plane field orientation. It is natural to have the critical field anisotropy in Figs. 5 (a) and (b) for the planar geometry of our experiment, however, the suppression pattern demonstrates non-monotonic behavior of the proximized superconductivity on the surface of altermagnet CrSb.

IV. DISCUSSION

As a result, we observe non-monotonic responses to an applied magnetic field in In-CrSb proximity devices, as well as a magnetic-field-induced asymmetry of the Josephson current in double In-CrSb-In junctions. In the latter case, the $dV/dI(B)$ curves are mirrored in respect to zero field for two magnetic field sweep directions, which is known for Josephson spin valves. For a single In-CrSb interface, the superconducting gap oscillates in magnetic field for both field orientations, before its full suppression.

Since indium is a conventional s-wave superconductor, the observed effects should mainly be associated with the specific properties of the proximized altermagnet CrSb.

The $dV/dI(B)$ curves reversal in respect to the zero field is not expected for conventional SFS junctions with a uniformly magnetized central layer, where remagnetiza-

tion can, at most, shift the position of the $I_c(B)$ pattern in magnetic field^{50,81}. We also verify, that there is no frozen flux in our solenoid for the field range in Fig. 2. Moreover, the flux could only shift the zero-resistance region in Fig. 2, so it is inconsistent with the $dV/dI(B)$ curves reversal and with the superconducting gap oscillations in Figs. 4 and 5.

By contrast, the observed behavior is a known fingerprint of Josephson spin valves^{50–57,63}. Whereas in conventional Josephson junctions the supercurrent is primarily modulated by the magnetic flux through the junction area, in JSV it is largely defined by the relative orientation of magnetic layers, giving rise to the $I_c(B)$ asymmetry and reversal.

It seems to be important that altermagnet CrSb exhibits both altermagnetic and topological features, including spin-polarized topological surface states^{72–74}. Due to spin-momentum locking, the topological surface states in CrSb are spin-polarized, in addition to the altermagnetic spin splitting in the bulk bands. Thus, In-CrSb-In junction should be viewed as containing at least two distinct (surface and bulk) magnetic phases. This naturally motivates a qualitative description of the In-CrSb-In junction in terms of the Josephson spin valve scenario. In our experiment, the strength of the spin-valve effect depends on the $\pi/2$ rotation of the magnetic field in Figs. 2 and 3, similarly to the interplay in magnetization between the altermagnetic bulk and the topological surface ones⁷⁴. Moreover, $dV/dI(B)$ hysteresis in Fig. 2 (a) is of approximately the same width as for unusual $M(H)$ diamagnetic hysteresis which has been attributed to the spin-polarized surface states⁷⁴.

The Josephson spin-valve behavior has recently been observed in Nb-Mn₃Ge-Nb junctions containing a single interlayer of the topological chiral antiferromagnet Mn₃Ge⁶³. The authors attributed this observation primarily to a proximity-induced, spin-polarised triplet supercurrent carried through Mn₃Ge. It was argued that the Berry-curvature-induced fictitious magnetic fields promote the spin-mixing and spin-rotation processes required for singlet-to-triplet pair conversion, thereby enabling long-range triplet supercurrent through a single chiral antiferromagnetic interlayer. At the same time, the role of topological surface states was not considered⁶³ for short Nb-Mn₃Ge-Nb junctions. While we agree that proximity-induced spin-polarized triplet supercurrent is an essential ingredient of the problem, we suggest that topological spin-polarized surface states play a central role in establishing the Josephson spin-valve behavior for long (2 μ m) In-CrSb-In junctions^{22–26}.

The Josephson diode effect typically accompanies Josephson spin-valve behavior^{29–31}, it can arise in superconductors hosting finite-momentum Cooper pairing^{30,31,83}, which can be favorable in altermagnets under certain conditions^{11,82–85}.

The finite-momentum Cooper pairing can also be responsible for non-monotonic response to an applied magnetic field for a single In-CrSb junction in Figs. 4, 5.

Among the various possible proximity-induced and intrinsic superconducting pairing states theoretically identified in altermagnets^{7,9–13}, finite-momentum pairing may emerge and give rise to a reentrant superconducting state as a function of the applied magnetic field⁸². For example, a non-monotonic field dependence of the critical temperature occurs after the transition into the Fulde-Ferrell-Larkin-Ovchinnikov (FFLO) state^{86,87} in hybrid layered SFN heterostructures. FFLO physics is based on finite-momentum Cooper pairing against a background of the Zeeman splitting, so it is fully compatible with the requirements for the Josephson diode effect^{30,31,83}. This might be a reason to have similar ≈ 13 mT period in Figs. 4, 5 and ≈ 13 mT shift of the zero-resistance region in Fig. 2 (b).

V. CONCLUSION

As a conclusion, we experimentally investigate charge transport in In-CrSb and In-CrSb-In proximity devices, which are formed as junctions between superconducting indium leads and thick single crystal flakes of altermag-

net CrSb. For double In-CrSb-In junctions, the obtained $dV/dI(B)$ curves are mirrored in respect to zero field for two magnetic field sweep directions, which is characteristic behavior of a Josephson spin valve. Also, we demonstrate Josephson diode effect by direct measurement of the critical current for two opposite directions in external magnetic field. We interpret these observations as a joint effect of the spin-polarized topological surface states and the altermagnetic spin splitting of the bulk bands in CrSb. For a single In-CrSb interface, the superconducting gap oscillates in magnetic field for both field orientations, which strongly resembles the transition into the Fulde-Ferrell-Larkin-Ovchinnikov state. The latter is based on finite-momentum Cooper pairing against a background of the Zeeman splitting, so it fully compatible with the requirements for the Josephson diode effect.

ACKNOWLEDGMENTS

We wish to thank S.S. Khasanov for X-ray sample characterization.

¹ N. P. Armitage, E. J. Mele, and Ashvin Vishwanath, "Weyl and Dirac semimetals in three-dimensional solids" *Rev. Mod. Phys.* 90, 15001 (2018)

² Hai-Yang Ma, Mengli Hu, Nana Li, Jianpeng Liu, Wang Yao, Jin-Feng Jia and Junwei Liu, *Nature Communications* 12, 2846 (2021)

³ Libor Šmejkal, Jairo Sinova, and Tomas Jungwirth, *Phys. Rev. X* 12, 031042 (2022)

⁴ Igor Mazin, *Phys. Rev. X* 12, 040002 (2022); 10.1103/PhysRevX.12.040002

⁵ J. Krempasky, L. Šmejkal, S.W. D'Souza, et al. *Nature* 626, 517–522 (2024)

⁶ Jabir Ali Ouassou, Arne Brataas, Jacob Linder, *Physical Review Letters* 131, 076003 (2023); <https://doi.org/10.1103/PhysRevLett.131.076003>

⁷ Igor I. Mazin, *AAAPS Bull.* 35, 18 (2025). <https://doi.org/10.1007/s43673-025-00158-6>

⁸ Sachchidanand Das, Dhavala Suri, Abhiram Soori, *J. Phys. : Condens. Matter* 35, 435302 (2023), <https://doi.org/10.1088/1361-648X/ace12>

⁹ Yuri Fukuya, Bo Lu, Keiji Yada, Yukio Tanaka, and Jorge Cayao, *J. Phys. : Condens. Matter* 37, 313003 (2025), <https://doi.org/10.1088/1361-648X/adf1cf>

¹⁰ Niclas Heinsdorf, and Marcel Franz, [arXiv:2509.03774](https://arxiv.org/abs/2509.03774)

¹¹ Song-Bo Zhang, Lun-Hui Hu, and Titus Neupert, *Nature Communications* 15, 1801 (2024).

¹² Yuri Fukaya, Kazuki Maeda, Keiji Yada, Jorge Cayao, Yukio Tanaka, and Bo Lu, *Phys. Rev. B* 111, 064502 (2025)

¹³ Ohidul Alam, Amartya Pal, Paramita Dutta, and Arijit Saha, [arXiv:2510.26894](https://arxiv.org/abs/2510.26894)

¹⁴ Qiang Cheng, Qing-Feng Sun, *Physical Review B* 109, 024517 (2024)

¹⁵ Michal Papaj, *Phys. Rev. B* 108, L060508 (2023)

¹⁶ Chi Sun, Arne Brataas, Jacob Linder, *Phys. Rev. B* 108, 054511 (2023)

¹⁷ Kazuki Maeda, Bo Lu, Keiji Yada, Yukio Tanaka, *J. Phys. Soc. Jpn.* 93, 114703 (2024)

¹⁸ Simran Chourasia, Aleksandr Svetogorov, Akashdeep Kamra, Wolfgang Belzig, *Phys. Rev. B* 111, 224503 (2025)

¹⁹ Yutaro Nagae, Andreas P. Schnyder, and Satoshi Ikegaya, *Phys. Rev. B* 111, L100507 (2025).

²⁰ D.Yu. Kazmin, V.D. Esin, Yu.S. Barash, A.V. Timonina, N.N. Kolesnikov, E.V. Deviatov, *Physica B: Condensed Matter*, 696, 416602 (2025)

²¹ B. Ghosh, D. Mondal, C.-N. Kuo, C. S. Lue, J. Nayak, J. Fujii, I. Vobornik, A. Politano, and A. Agarwal, *Phys. Rev. B* 100, 195134 (2019).

²² J. H. Lee, G.-H. Lee, J. Park, J. Lee, S.-G. Nam, Y.-S. Shin, J. S. Kim, and H.-J. Lee, *Nano Lett.* 14, 5029 (2014).

²³ A. Kononov, O. O. Shvetsov, S. V. Egorov, A. V. Timonina, N. N. Kolesnikov, and E. V. Deviatov, *Europhys. Lett.* 122, 27004 (2018).

²⁴ C. Huang, B. T. Zhou, H. Zhang, B. Yang, R. Liu, H. Wang, Y. Wan, K. Huang, Z. Liao, E. Zhang, S. Liu, Q. Deng, Y. Chen, X. Han, J. Zou, X. Lin, Z. Han, Y. Wang, K. Tuen Law & F. Xiu, *Nat. Comm.* 10, 2217 (2019).

²⁵ O. O. Shvetsov, V. D. Esin, Yu. S. Barash, A. V. Timonina, N. N. Kolesnikov, and E. V. Deviatov, *Phys. Rev. B* 101, 035304 (2020).

²⁶ Y. Wang, S. Yang, P. K. Sivakumar, B. R. Ortiz, S. M. L. Teicher, H. Wu, A. K. Srivastava, C. Garg, D. Liu, S. S. P. Parkin, E. S. Toberer, T. McQueen, S. D. Wilson, M. N. Ali, [arXiv:2012.05898](https://arxiv.org/abs/2012.05898).

²⁷ Daniil S. Antonenko, Rafael M. Fernandes, Jorn W. F. Venderbos, *Phys. Rev. Lett.* 134, 096703 (2025)

²⁸ Rafael M. Fernandes, Vanuildo S. de Carvalho, Turan Birol, Rodrigo G. Pereira, *Phys. Rev. B* 109, 024404

(2024).

²⁹ O. O. Shvetsov, Yu. S. Barash, A. V. Timonina, N. N. Kolesnikov, E. V. Deviatov, *JETP Letters*, 115, 267–275 (2022). DOI: 10.1134/S0021364022100101

³⁰ Banabir Pal, Anirban Chakraborty, Pranava K. Sivakumar, Margarita Davydova, Ajesh K. Gopi, Avanindra K. Pandeya, Jonas A. Krieger, Yang Zhang, Mihir Date, Sailong Ju, Noah Yuan, Niels B. M. Schröter, Liang Fu and Stuart S. P. Parkin, *Nat. Phys.* 18, 1228 (2022). <https://doi.org/10.1038/s41567-022-01699-5>

³¹ Varnava D. Esin, Oleg O. Shvetsov, Anna V. Timonina, Nikolai N. Kolesnikov and Eduard V. Deviatov, *Nanomaterials* 12(23), 4114 (2022). <https://doi.org/10.3390/nano12234114>

³² Y Zhang, Y Gu, P Li, J Hu, K Jiang, *Phys. Rev. X* 12, 041013 (2022).

³³ Andreas Costa, Jaroslav Fabian, and Denis Kochan, *Phys. Rev. B* 108, 054522 (2023).

³⁴ Muhammad Nadeem, Michael S. Fuhrer, and Xiaolin Wang, *Nat. Rev. Phys.* 5, 558–577 (2023).

³⁵ P. J. W. Moll, and V. B. Geshkenbein, *Nat. Phys.* 19, 1379–1380 (2023).

³⁶ Naoto Nagaosa, and Youichi Yanase, *Annual Review Condensed Matter Physics*. 15, 63–83 (2024).

³⁷ J. Ma, R. Zhan, and X. Lin, *Adv. Phys. Res.* 4, 2400180 (2025).

³⁸ Daniel Shaffer, Alex Levchenko, arXiv:2510.25864.

³⁹ Akito Daido, Yuhei Ikeda, Youichi Yanase, *Phys. Rev. Lett.* 128, 037001 (2022) DOI: <https://doi.org/10.1103/PhysRevLett.128.037001>

⁴⁰ Noah F. Q. Yuan, Liang Fu, *PNAS* 119, e2119548119, (2022) <https://doi.org/10.1073/pnas.2119548119>

⁴¹ James Jun He, Yukio Tanaka, Naoto Nagaosa, *New J. Phys.* 24 053014 (2022) <https://doi.org/10.1088/1367-2630/ac6766>

⁴² A. Buzdin, *Phys. Rev. Lett.* 101, 107005 (2008).

⁴³ F. Konschelle and A. Buzdin, *Phys. Rev. Lett.* 102, 017001 (2009); *Phys. Rev. Lett.* 123, 169901(E) (2019).

⁴⁴ I. Kulagina and J. Linder, *Phys. Rev. B* 90, 054504 (2014).

⁴⁵ M. A. Silaev, I. V. Tokatly, and F. S. Bergeret, *Phys. Rev. B* 95, 184508 (2017).

⁴⁶ Yu. M. Shukrinov, I. R. Rahmonov, K. Sengupta, and A. Buzdin, *Appl. Phys. Lett.* 110, 182407 (2017).

⁴⁷ Ya-Jun Wei, and J. Wang, *EPL* 148, 56003 (2024).

⁴⁸ M. Tsoi, A. G. M. Jansen, J. Bass, W.-C. Chiang, M. Seck, V. Tsoi, and P. Wyder, *Phys. Rev. Lett.* 80, 4281 (1998).

⁴⁹ E. B. Myers, D. C. Ralph, J. A. Katine, R. N. Louie, and R. A. Buhrman, *Science* 285, 867 (1999).

⁵⁰ N. Banerjee, J. W. A. Robinson, M. G. Blamire, *Nat. Commun.* 5, 4771 (2014).

⁵¹ E. C. Gingrich, B. M. Niedzielski, J. A. Glick, Y. Wang, D. L. Miller, R. Loloei, W. P. Pratt Jr., N. O. Birge, *Nat. Phys.* 12, 564 (2016).

⁵² Y. Zhu, A. Pal, M. Blamire, et al. *Nature Mater* 16, 195 (2017).

⁵³ B. M. Niedzielski, T. J. Bertus, J. A. Glick, R. Loloei, W. P. Pratt Jr., and N. O. Birge *Phys. Rev. B* 97, 024517 (2018).

⁵⁴ N. Satchell, P. M. Shepley, M. Algarni, M. Vaughan, E. Darwin, M. Ali, M. C. Rosamond, L. Chen, E. H. Linfield, B. J. Hickey, and G. Burnell, *Appl. Phys. Lett.* 116, 022601 (2020).

⁵⁵ O. M. Kapran, A. Iovan, T. Golod, V. M. Krasnov, *Phys. Rev. Research* 2, 013167 (2020).

⁵⁶ Yu He, Jiaxu Li, Qiusha Wang, Hisakazu Matsuki, and Guang Yang, *Adv Devices Instrum.*, 4, 0035 (2023)

⁵⁷ Norman O. Birge, and Nathan Satchell, *APL Mater.* 12, 041105 (2024)

⁵⁸ T. Yu. Karminskaya, M. Yu. Kupriyanov, and A. A. Golubov, *JETP Letters* 87, 570 (2008).

⁵⁹ V. D. Esin, D. N. Borisenko, A. V. Timonina, N. N. Kolesnikov, and E. V. Deviatov, *Phys. Rev. B* 101, 155309 (2020).

⁶⁰ V. D. Esin, A. V. Timonina, N. N. Kolesnikov, E. V. Deviatov, *Journal of Magnetism and Magnetic Materials*, 540, 168488 (2021). <https://doi.org/10.1016/j.jmmm.2021.168488>

⁶¹ J. Tian, I. Miotkowski, S. Hong, Y. P. Chen, *Sci. Rep.* 5, 14293 (2015).

⁶² A.A. Avakyants, V.D. Esin, D.Yu. Kazmin, N.N. Orlova, A.V. Timonina, N.N. Kolesnikov, and E.V. Deviatov, *JETP Letters*, Vol. 121, 727 (2025). DOI: 10.31857/S0370274X25050099

⁶³ Kun-Rok Jeon, Binoy Krishna Hazra, Jae-Keun Kim, Jae-Chun Jeon, Hyeon Han, Holger L. Meyerheim, Takis Kontos, Audrey Cottet, Stuart S. P. Parkin, *Nat. Nanotechnol.* 18, 747–753 (2023)

⁶⁴ Sayan Banerjee, and Mathias S. Scheurer, *Phys. Rev. B* 110, 024503 (2024).

⁶⁵ Lovy Sharma, Manisha Thakurathi, *Phys. Rev. B* 112, 104506 (2025).

⁶⁶ Debmalya Chakraborty, Annica M. Black-Schaffer, *Phys. Rev. Lett.* 135, 026001 (2025).

⁶⁷ S. Reimers, L. Odenbreit, P. Constantinou, L. Šmejkal, A. B. Hellenes et al. Direct observation of altermagnetic band splitting in CrSb thin films. *Nat Commun* 15, 2116 (2024). <https://doi.org/10.1038/s41467-024-46476-5>

⁶⁸ Satoru Hayami and Hiroaki Kusunose, "Essential role of the anisotropic magnetic dipole in the anomalous Hall effect" *Phys. Rev. B* 103, L180407 (2021).

⁶⁹ A. Hariki, A. Dal Din, O. J. Amin, T. Yamaguchi, A. Badura, D. Kriegner, K. W. Edmonds, R. P. Campion, P. Wadley, D. Backes, L. S. I. Veiga, S. S. Dhesi, G. Springholz, L. Smejkal, K. Vyborny, T. Jungwirth, J. Kunes, "X-Ray Magnetic Circular Dichroism in Altermagnetic α -MnTe" *Phys. Rev. Lett.* 132, 176701 (2024)

⁷⁰ M. Hajlaoui, S.W. D'Souza, L. Smejkal, D. Kriegner, G. Krizman, T. Zakušylo, N. Olszowska, O. Caha, J. Michalička, A. Marmodoro, K. Výborný, A. Ernst, M. Cinchetti, J. Minar, T. Jungwirth, G. Springholz, "Temperature Dependence of Relativistic Valence Band Splitting Induced by an Altermagnetic Phase Transition" *Adv. Mater.* 36, 2314076 (2024)

⁷¹ G. Yang, Zh. Li, S. Yang, J. Li, H. Zheng, W. Zhu, Z. Pan, Y. Xu, S. Cao, W. Zhao, A. Jana, J. Zhang, M. Ye, Yu Song, L.-H. Hu, L. Yang, J. Fujii, I. Vobornik, M. Shi, H. Yuan, Y. Zhang, Y. Xu and Y. Liu, Three-dimensional mapping of the altermagnetic spin splitting in CrSb, *Nature Communications* Vol. 16, 1442, pp. 1 (2025)

⁷² Wenlong Lu, Shiyu Feng, Yuzhi Wang, Dong Chen, Zihan Lin, Xin Liang, Siyuan Liu, Wanxiang Feng, Kohei Yamagami, Junwei Liu, Claudia Felser, Quansheng Wu and Junzhang Ma, Signature of Topological Surface Bands in Altermagnetic Weyl Semimetal CrSb, *Nano Letters*, Vol 25, 18, pp. 7343, (2025)

⁷³ Cong Li, Mengli Hu, Zhilin Li, Balasubramanian Thagarajan, Yang Wang, Wanyu Chen, Mats Leandersson,

Craig Polley, Cosma Fulga, Maia G. Vergniory, Oleg Jansson, Timur Kim, Oscar Tjernberg, Jeroen van den Brink, Topological Weyl altermagnetism in CrSb, Communications Physics 8, 311, pp. 1 (2025)

⁷⁴ N.N. Orlova, A.A. Avakyants, V.D. Esin, A.V. Timonina, N.N. Kolesnikov, and E.V. Deviatov, arXiv: 2512.11344

⁷⁵ O.O. Shvetsov, A. Kononov, A.V. Timonina, N.N. Kolesnikov, E.V. Deviatov, JETP Letters, 107, 774 (2018).

⁷⁶ V. D. Esin, D. Yu. Kazmin, Yu. S. Barash, A. V. Timonina, N. N. Kolesnikov, E. V. Deviatov, JETP Letters, 118, 847 (2023). <https://doi.org/10.1134/S0021364023603329>

⁷⁷ A. F. Andreev, Soviet Physics JETP 19, 1228 (1964).

⁷⁸ M. Tinkham, Introduction to Superconductivity (2d ed., McGraw-Hill, New York, 1996).

⁷⁹ P. Scharnhorst, Phys. Rev. B 1, 4295 (1970).

⁸⁰ A. M. Toxen Phys. Rev. 123, 442 (1961).

⁸¹ R. S. Keizer, S. T. B. Goennenwein, T. M. Klapwijk, G. Miao, G. Xiao, A. Gupta, Nature 439, 825 (2006).

⁸² Debmalya Chakraborty, Annica M. Black-Schaffer, Phys. Rev. B 110, L060508 (2024).

⁸³ Noah F. Q. Yuan, and Liang Fu, PNAS 119, e2119548119 (2022).

⁸⁴ GiBaik Sim, and Johannes Knolle, Phys. Rev. B 112, L020502 (2025)

⁸⁵ Kohei Mukasa, and Yusuke Masaki, J. Phys. Soc. Jpn. 94, 064705 (2025)

⁸⁶ S. V. Mironov, A. V. Samokhvalov, A. I. Buzdin, and A. S. Mel'nikov, JETP Letters 113, 92 (2021).

⁸⁷ A S Mel'nikov, S V Mironov, A V Samokhvalov, A I Buzdin, Physics-Uspekhi 65, 1248 (2022).